Scientia Iranica A (2015) 22(5), 1643–1660

Sharif University of Technology
Scientia Iranica
Transactions A: Civil Engineering
www.scientiairanica.com

Use of hyper-elasticity in anisotropic clay plasticity models

A. Lashkari* **and M. Mahboubi**

Department of Civil & Environmental Engineering, Shiraz University of Technology, Shiraz, Iran.

Received 8 July 2013; received in revised form 12 August 2014; accepted 6 December 2014

KEYWORDS
Clay;
Anisotropy;
Elasticity;
Gibbs free energy;
Plasticity.

Abstract. In conventional elastic-plastic constitutive models for clays, elastic strains are usually calculated by isotropic hypo-elastic models. However, this class of elasticity has two major deficiencies: (a) It ignores the influence of shear stress-induced anisotropy and; (b) It does not conserve energy. Another class of the elasticity theory, the so-called hyper-elasticity theory, is capable of eliminating both deficiencies simultaneously. In this study, constitutive equations of a recently proposed elastic-plastic platform for clays named SANICLAY are generalized in order to enable it to consider the possibility of the anisotropic response in the elastic domain. The generalized formulation allows shear-volumetric coupling not existing in the basic platform. Then, the elastic moduli obtained from a hyper-elastic model are implemented within the generalized SANICLAY formulation. The refined model predictions are directly compared with the experimental data of various clays. It is shown that more realistic stress paths are achieved from the refined model.

1. Introduction

During the last decades, a considerable amount of experimental studies regarding the mechanical behavior of cohesive soils was published in the literature [1-7]. Besides, a large number of elastic-plastic constitutive models for clayey soils have been introduced [8-18] among which there exist complex constitutive models that can realistically predict soil behavior under various stress paths (e.g. [11,15]). Nevertheless, for solving boundary value problems, the simpler constitutive models that succeeded to set a balance between simplicity and correctness of predictions are always appealed. In this regard, the Modified Cam-Clay (MCC) family, an extended class of constitutive models developed based on the theory of plastic work hardening, has been widely used in the literature. Essential advantages of this family are: (a) They are established based on the critical state soil mechanics; (b) They use a small number of parameters with clear physical meanings. These parameters can be determined using conventional equipment in soil mechanics laboratory; and (c) The performance of the original frame (i.e., the MCC model) has been thoroughly evaluated within the last 45 years [11]. The MCC model was originally proposed by Roscoe and Burland [8]. Dafalias [9] reported a formulation for the extension of MCC from isotropic to anisotropic response. Using the critical state soil mechanics concepts in conjunction with rotational hardening and non-associated flow rule, Newson and Davies [10] proposed an extension to MCC known as CARMEL. Assuming an associated flow rule, Wheeler et al. [12] and Karstunen et al. [13] introduced the S-Clay1 as an anisotropic generalization of the MCC model. Unlike previous models (i.e., [8-11]), evolution of the yield function orientation in S-Clay1 is controlled by both plastic volumetric and plastic deviator strains. Employing a non-associated flow rule,

*. *Corresponding author.*
E-mail addresses: lashkari@sutech.ac.ir and lashkari_ali@hamyar.net (A. Lashkari)

rotational/distortional hardening, and the so-called attractor concept for asymptotic states, Dafalias et al. [16] introduced the SANICLAY model. Unlike other members of the MCC family, this model is capable of simulating the peak point observed in the deviator stress of highly anisotropically consolidated samples subjected to undrained shear. Recently, Papadimitriou et al. [17] have studied the influence of yield function shape on the simulative capacity of SANICLAY. More recently, Taiebat et al. [18] suggested a modified SANICLAY model that is capable of considering destructuration. It is worthy to note that the difference between the models named above (i.e., [8-10,12-14,16]) returns back essentially to constitutive equations describing the evolution of hardening internal variables and flow rule.

Elastic strains in the majority of clay constitutive models are conventionally calculated using hypo-elastic models (e.g., [19-21]). However, it has been shown that hypo-elasticity theories do not conserve energy. This drawback eventually leads to irreversibility of elastic strains that is a flaw [22,23]. To avoid this deficiency, the application of another class of the elasticity theory, the so-called hyper-elasticity, is essential. In this class of the elasticity, constitutive equations for calculation of elastic strain components are obtained from partial differentiation of the Gibbs/Helmholtz free energy functions. This approach guarantees to conserve energy in every closed-loop stress path. Besides, Einav & Puzrin [24] have shown that soil hyper-elastic models can predict the shear stress-induced anisotropy in a natural unforced way. In the recent years, few hyper-elastic models have been introduced for reconstituted clays [23-25].

When subjected to shear stress, both the yield and the plastic flow mechanisms in the SANICLAY grow to be increasingly anisotropic. However, hypo-elastic constitutive equations describing the elastic response of the soil always remain isotropic that is not realistic [26,27]. In this study, the most general form of constitutive equations for anisotropic response of soils is implemented within the SANICLAY platform. Then, the elastic moduli based on the Gibbs energy function of Einav & Puzrin [24] are obtained and employed in the SANICLAY model. The modified model conserves energy for the elastic portion of the behavior. Besides, it is shown that the refined model provides reasonable predictions for the undrained behavior of highly over-consolidated clays.

2. Non-linear elasticity for clays

Unlike metals, the elastic moduli of soils are pressure dependent. Further, in reconstituted samples, elastic moduli become gradually anisotropic alongside with shear stress. Generally, the elastic response of soils in triaxial space is described by [26-28]:

$$\dot{p} = K\dot{\varepsilon}_v^e + J\dot{\varepsilon}_q^e; \qquad \dot{q} = J\dot{\varepsilon}_v^e + 3G\dot{\varepsilon}_q^e, \tag{1}$$

where, p and q are mean principal effective stress and deviator stress. K, G, and J are, respectively, the elastic bulk, shear, and coupling moduli. ε_v^e and ε_q^e are elastic volumetric and elastic deviator strains, respectively.

For isotropic media, $J = 0$ and Eq. (1) is reduced to:

$$\dot{p} = K\dot{\varepsilon}_v^e; \qquad \dot{q} = 3G\dot{\varepsilon}_q^e. \tag{2}$$

From Eq. (2), it can be observed that the change in the mean principal effective stress is only related to the change in volumetric elastic strain in isotropic elastic soils. In a similar fashion, variation of the deviator stress is just affected by the rate of deviator strain. In the opposite side, $J \neq 0$ holds for anisotropic soils. The presence of non-zero J terms in Eq. (1) causes the so-called shear-volumetric coupling effect to happen in which $\dot{p}$ and $\dot{q}$ are also dependent on both $\dot{\varepsilon}_v^e$ and $\dot{\varepsilon}_q^e$ [26-28].

2.1. Non-linear isotropic hypo-elasticity for clays [19-21]

In isotropic compression (consolidation) of reconstituted clays, void ratio varies almost in a linear manner when it is drawn in the e-ln(p) plane. In theoretical and practical applications, it is very common to calculate the elastic shear and bulk moduli of clays through the following hypo-elastic constitutive equations [19-21]:

$$K = \frac{(1+e_{\text{in}})}{k}p; \qquad G = \frac{3}{2}\left(\frac{1-2v}{1+v}\right)K, \tag{3}$$

where, e_{in}, ν and k are, respectively, initial void ratio, Poisson's ratio, and the slope of unloading/re-loading curve in e-ln(p) plane. In this elasticity model, $J = 0$ is a result of the assumption of isotropy. The above definition for K leads to the linear change in void ratio in e-ln(p) plane under isotropic compression. Furthermore, G is directly related to K by means of a constant Poisson's ratio. The above elasticity belongs to the hypo-elasticity family and hence, it does not conserve energy in a general closed-loop stress path [22-24]. It has been shown that the application of hypo-elasticity may lead to unrealistic design in a number of geotechnical engineering problems such as tunnels and excavations [24]. In these cases, elastic unloading, in conjunction with the reduction of mean principal effective stress, highlights the significance of hyper-elasticity [23]. Generally, hyper-elasticity necessitates a coupling effect between shear and volumetric strains. As a consequence, the balance between the volumetric elastic and plastic strains in constant volume shear can lead to a remarkable change in the elastic-plastic

regime of behavior [24]. For instance, Einav & Puzrin [24] conducted elasto-plastic numerical studies on the engineering behavior of tunnels constructed in over-consolidated clays under undrained condition. In their analyses, the vertical settlements obtained from the hyper-elastic theory are larger than those of the conventional hypo-elastic theory (i.e., Eqs. (3)) when the stress state is located within the yield function. On the other hand, the hyper-elasticity in conjunction with the conventional plasticity dictates larger stress components at the yield state compared to a similar analysis in combination with hypo-elasticity. As a consequence, plastic settlements in the elasto-plastic regime of behavior are usually over-predicted when the elastic branch of behavior is simulated using a hypo-elastic model [24].

2.2. A non-linear hyper-elasticity model for clays [24]

In the hyper-elasticity theory proposed by Einav & Puzrin [24], elastic strains are calculated by means of the following Gibbs free energy function, $\Gamma(p,q)$, defined by:

$$\Gamma(p,q) = \bar{k}p\left(\ln(\frac{p}{p_{\text{in}}}) - 1\right) + \frac{q^2}{6\bar{G}p_{\text{ref}}}\left(\frac{p_{\text{ref}}}{p}\right)^{\theta} - \frac{q_{\text{in}}(2qp_{\text{in}} - \theta q_{\text{in}}p)}{6\bar{G}p_{\text{ref}}^2}\left(\frac{p_{\text{ref}}}{p_{\text{in}}}\right)^{\theta+1}, \quad (4)$$

where, $\bar{G}$, θ and $\bar{k}$ are the hyper-elastic model parameters and $p_{\text{ref}} = 100$ kPa is a normalizing pressure. The physical meanings behind $\bar{G}$, θ and $\bar{k}$ are discussed after Eqs. (9). A 3-D view of free strain energy of Eq. (4) is shown in Figure 1. The stored energy should be zero at $(p,q) = (0,0)$ and hence, the surface shown in Figure 1 passes through the origin. Besides, soil elastic moduli must be zero at $p = 0$. As a consequence, the Gibbs free energy surface has a vertical asymptote at $p = 0$ plane.

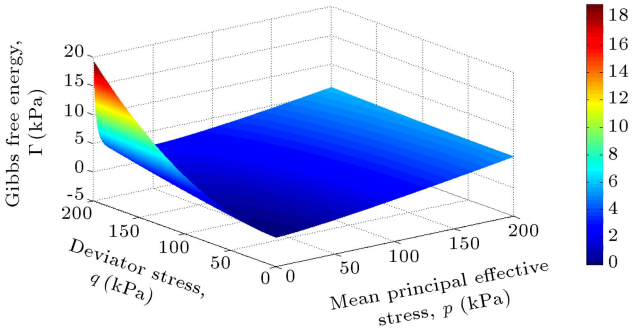

Figure 1. A 3-D representation of Gibbs free strain energy function of Einav & Puzrin [24] whose mathematical expression is presented in Eq. (4) (parameters are given in Table 2 for LCT clay and $p_{\text{in}} = 1$ kPa).

Using Eq. (4), elastic strain components become:

$$\varepsilon_v^e = \frac{\partial\Gamma(p,q)}{\partial p} = \bar{k}\ln\left(\frac{p}{p_{\text{in}}}\right) - \frac{\theta}{6\bar{G}}\left(\eta^2\left(\frac{p_{\text{ref}}}{p}\right)^{\theta-1} - \eta_{\text{in}}^2\left(\frac{p_{\text{ref}}}{p_{\text{in}}}\right)^{\theta-1}\right),$$

$$\varepsilon_q^e = \frac{\partial\Gamma(p,q)}{\partial q} = \frac{1}{3\bar{G}p_{\text{ref}}^{1-\theta}}\left(\frac{q}{p^{\theta}} - \frac{q_{\text{in}}}{p_{\text{in}}^{\theta}}\right), \quad (5)$$

where, $\eta(= q/p)$ is stress ratio and $\eta_{\text{in}} = q_{\text{in}}/p_{\text{in}}$. Considering Eq. (5), both volumetric and deviator elastic strains are zero when $p = p_{\text{in}}$ and $q = q_{\text{in}}$.

Further differentiation of Eq. (5) yields the rate form of elastic strains:

$$\dot{\varepsilon}_v^e = \frac{\partial\Gamma^2(p,q)}{\partial p\partial p}\dot{p} + \frac{\partial\Gamma^2(p,q)}{\partial p\partial q}\dot{q} = \left(\frac{\bar{k}}{p} + \frac{\theta(\theta+1)}{6\bar{G}_{p\text{ref}}}\eta^2\left(\frac{p_{\text{ref}}}{p}\right)^{\theta}\right)\dot{p} - \left(\frac{\theta}{3\bar{G}p_{\text{ref}}}\eta\left(\frac{p_{\text{ref}}}{p}\right)^{\theta}\right)\dot{q}$$

$$\dot{\varepsilon}_q^e = \frac{\partial\Gamma^2(p,q)}{\partial q\partial p}\dot{p} + \frac{\partial\Gamma^2(p,q)}{\partial q\partial q}\dot{q} = -\left(\frac{\theta}{3\bar{G}p_{\text{ref}}}\eta\left(\frac{p_{\text{ref}}}{p}\right)^{\theta}\right)\dot{p} + \left(\frac{1}{3\bar{G}p_{\text{ref}}}\left(\frac{p_{\text{ref}}}{p}\right)^{\theta}\right)\dot{q}. \quad (6)$$

Solving Eq. (6) with respect to $\dot{p}$ and $\dot{q}$ gives:

$$\dot{p} = \frac{1}{1 - \frac{\theta(\theta-1)}{6\bar{G}\bar{k}}\eta^2(\frac{p}{p_{\text{ref}}})^{1-\theta}}\left(\left(\frac{p}{\bar{k}}\right)\dot{\varepsilon}_v^e + \left(\theta\eta\frac{p}{\bar{k}}\right)\dot{\varepsilon}_q^e\right),$$

$$\dot{q} = \frac{1}{1 - \frac{\theta(\theta-1)}{6\bar{G}\bar{k}}\eta^2(\frac{p}{p_{\text{ref}}})^{1-\theta}}\left(\left(\theta\eta\frac{p}{\bar{k}}\right)\dot{\varepsilon}_v^e + \left(3\bar{G}p_{\text{ref}}\left(\frac{p}{p_{\text{ref}}}\right)^{\theta} + \frac{\theta(\theta+1)}{2}\eta^2\frac{p}{\bar{k}}\right)\dot{\varepsilon}_q^e\right). \quad (7)$$

Now, one can find the elastic moduli by comparing Eqs. (1) and (7):

$$G = \frac{\bar{G}p_{\text{ref}}\left(\frac{p}{p_{\text{ref}}}\right)^{\theta} + \frac{\theta(\theta+1)}{6}\eta^2\frac{p}{\bar{k}}}{1 - \frac{\theta(\theta-1)}{6\bar{G}\bar{k}}\eta^2\left(\frac{p}{p_{\text{ref}}}\right)^{1-\theta}},$$

$$K = \frac{\frac{p}{\bar{k}}}{1 - \frac{\theta(\theta-1)}{6\bar{G}\bar{k}}\eta^2\left(\frac{p}{p_{\text{ref}}}\right)^{1-\theta}},$$

$$J = \frac{\theta\eta\frac{p}{k}}{1 - \frac{\theta(\theta-1)}{6\bar{G}\bar{k}}\eta^2\left(\frac{p}{p_{\text{ref}}}\right)^{1-\theta}} = \theta\eta K. \tag{8}$$

For isotropic stress condition (i.e., $p \neq 0$; $q = 0$ and then $\eta = 0$), Eq. (8) is reduced to:

$$G = \bar{G}p_{\text{ref}}\left(\frac{p}{p_{\text{ref}}}\right)^{\theta}, \qquad K = \frac{p}{\bar{k}} \qquad J = 0. \tag{9}$$

By setting $\bar{k} = \frac{k}{1+e_{\text{in}}}$, the hyper-elasticity of Einav & Puzrin [24] becomes capable of replicating the linear variation of void ratio in the e-ln(p) plane under isotropic compression (consolidation). According to Eqs. (9), $\bar{G}$ is a non-dimensional parameter that scales the magnitude of the elastic shear modulus at extremely low shear stress levels. The non-linear manner of the change in G with p is defined through the exponent θ, and, k is the slope of unloading/reloading paths in the e-ln(p) plane.

2.3. Comparison of elasticity models in a closed-loop elastic stress path

For a closed-loop stress path, elastic strains predicted by the hypo-elastic model of references [19-21] are shown through parts (b)-(e) of Figure 2. Considering parts (c) and (e) of Figure 2, it can easily be found that deviator elastic strain is irreversible ($(\varepsilon_q^e)_A \neq (\varepsilon_q^e)_E$) in the closed-loop stress path $A \rightarrow B \rightarrow C \rightarrow D \rightarrow E(= A)$. For the same stress path, elastic strains obtained from the hyper-elastic model of Einav & Puzrin [24] are illustrated in parts (b)-(e) of Figure 3. It can be observed that in all cases, both volumetric and deviator elastic strains calculated by the hyper-elastic model are reversible upon the complete reversal of the stress.

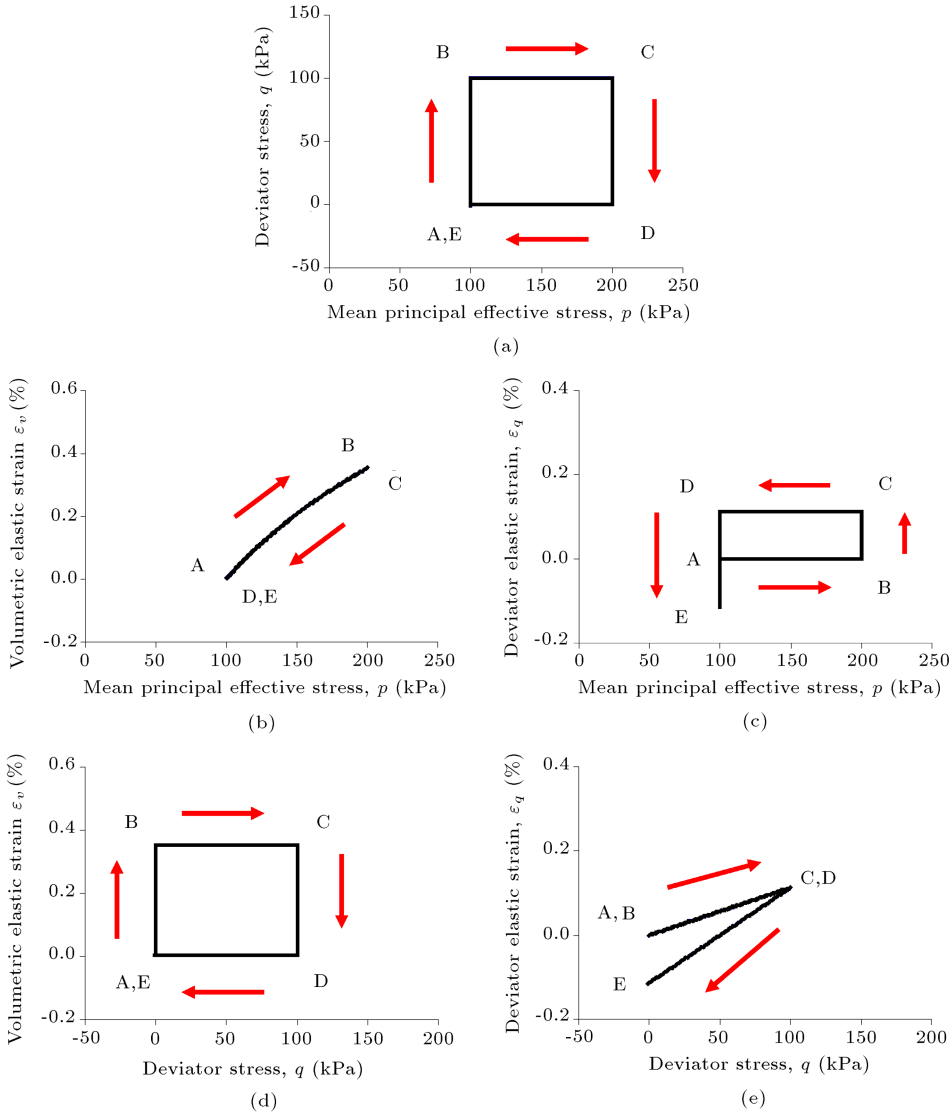

Figure 2. Numerical studies of elastic strains calculated by the hypo-elastic model [19-21] during a closed-loop stress path ($e_{\text{in}} = 0.769$, $k = 0.009$, $\upsilon = 0.20$, and $p_{\text{ref}} = 100$ kPa): (a) Demonstration of the stress path; (b) ε_v vs. p; (c) ε_q vs. p; (d) ε_v vs. q; and (e) ε_q vs. q.

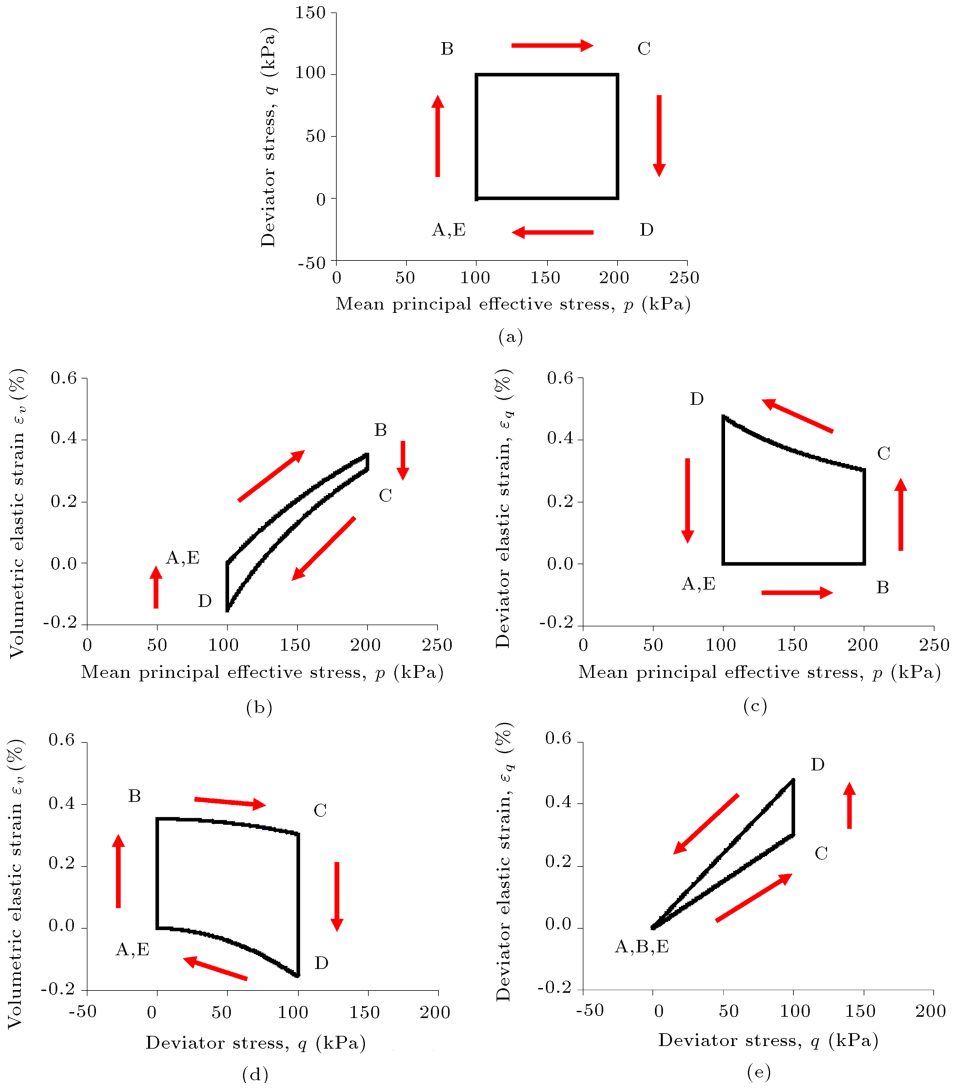

Figure 3. Numerical studies of elastic strains calculated by the hypo-elastic model [24] during a closed-loop stress path ($e_{\text{in}} = 0.769$, $k = 0.009$; $\bar{G} = 70$, $n = 0.65$, and $p_{\text{ref}} = 100$ kPa): (a) Demonstration of the stress path; (b) ε_v vs. p; (c) ε_q vs. p; (d) ε_v vs. q; and (e) ε_q vs. q.

Comparison of the corresponding parts of Figures 2 and 3 reveals that a noticeable difference between the manners of elastic strains generated in each fraction of the closed-loop stress path exists. Prevention of drainage in constant volume (i.e., undrained) stress paths dictates a balance between the volumetric elastic and volumetric plastic strain rates (i.e., $\dot{\varepsilon}_v^p = -\dot{\varepsilon}_v^e$ because $\dot{\varepsilon}_v^e + \dot{\varepsilon}_v^p = \dot{\varepsilon}_v = 0$). Considering the latter point, the diversity in patterns of elastic strains illustrated in Figures 2 and 3 necessitates a distinction between the generated plastic strains and the evolution of hardening variables in undrained stress paths.

3. Formulation of a simple anisotropic elastic-plastic model for clays

Recently, Dafalias et al. [16] introduced a Simple ANIsotropic CLAY model, SANICLAY, as an extension of the MCC model. The model is based on the critical state soil mechanics and non-associated flow rule. Thus, the mathematical expressions of the yield and plastic potential functions are not identical. The sizes of the yield and plastic potential functions are changed as a result of isotropic hardening. Further, they may be subjected to rotational/distortional hardening as a direct consequence of the stress-induced fabric anisotropy (see Figure 4). Through Eqs. (10)-(17), a brief review of the formulation of the SANICLAY model is presented in Table 1. In its original form with isotropic hypo-elasticity (see Section 2.1), SANICLAY has 8 parameters (i.e., M_c, M_e, N, λ, k, ν, C, x) that may be determined systematically (see [16]). M_c and M_e are slopes of critical state lines drawn in the $q-p$ plane under the compression and extension modes of triaxial, respectively. N is a parameter in the yield function that plays the same role as M in the

Table 1. Outline of the SANICLAY formulation [16].

Description	Constitutive equation	Parameter(s)	Equation number
Yield function	$f=(q-p\beta)^2-(N^2-\beta^2)p(p_0-p)=0$	N	(10)
Plastic potential function	$g=(q-p\alpha)^2-(M^2-\alpha^2)p(p_\alpha-p)=0$	$M(M_c \text{ or } M_e)$	(11)
Evolution of internal variables	$\dot{p}_0=\langle\Lambda\rangle\bar{p_0}=\langle\Lambda\rangle\left(\frac{1+e_{in}}{\lambda-k}\right)p_0\left(\frac{\partial g}{\partial p}\right)$	λ, k	(12)
	$\dot{\alpha}=\langle\Lambda\rangle\bar{\alpha}=\langle\Lambda\rangle\left(\frac{1+e_{in}}{\lambda-k}\right)C\left(\frac{p}{p_0}\right)^2\left\|\frac{\partial g}{\partial p}\right\|\|\eta-x\alpha\|(\alpha^b-\alpha)$ $\eta/x>\alpha\rightarrow\alpha^b=M_c;\quad \eta/x<\alpha\rightarrow\alpha^b=-M_e$	$\lambda, k, C, x, M_c, M_e$	(13)
	$\dot{\beta}=\langle\Lambda\rangle\bar{\beta}=\langle\Lambda\rangle\left(\frac{1+e_{in}}{\lambda-k}\right)C\left(\frac{p}{p_0}\right)^2\left\|\frac{\partial g}{\partial p}\right\|\|\eta-\beta\|(\beta^b-\beta)$ $\eta>\beta\rightarrow\beta^b=N;\quad \eta/\beta\rightarrow\beta^b=-N$	λ, k, C, N	(14)
Plastic hardening modulus	$K_p=-\left(\frac{\partial f}{\partial p_0}\bar{p_0}+\frac{\partial f}{\partial\beta}\bar{\beta}\right)=p\left[(N^2-\beta^2)\bar{p_0}+2(q-p_0\beta)\bar{\beta}\right]$	–	(15)
Loading index	$\Lambda=\frac{1}{K_p}\left(\frac{\partial f}{\partial p}\dot{p}+\frac{\partial f}{\partial q}\dot{q}\right)=\frac{1}{K_p}p\left[(N^2-\eta^2)\dot{p}+2(\eta-\beta)\dot{q}\right]$	–	(16)
Volumetric and deviator plastic strain rates	$\dot{\varepsilon}_v^p=\langle\Lambda\rangle\frac{\partial g}{\partial p}=\langle\Lambda\rangle p(M^2-\eta^2);\quad \dot{\varepsilon}_q^p=\langle\Lambda\rangle\frac{\partial g}{\partial q}=2\langle\Lambda\rangle p(\eta-\alpha)$	–	(17)

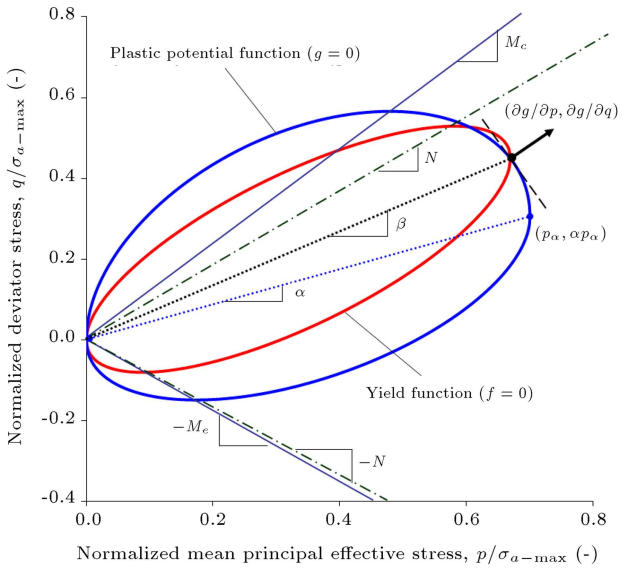

Figure 4. Schematic view of yield and plastic potential functions in SANICLAY [16].

plastic potential function. λ and k are, respectively, the slopes of normal compression and unloading/reloading lines depicted in the e-ln(p) plane. ν is the Poisson's ratio. C is a parameter that controls the pace of rotation of yield and plastic potential functions. For samples anisotropically consolidated in the compression side, an increase in C leads to a tendency to contraction for subsequent undrained towards the extension side. Finally, x provides a bound for rotation of the plastic potential function. Setting $p_\alpha=p_0$, $N=M$, $\alpha=0$ and $\beta=0$, the SANICLAY model of Dafalias et al. [16] is simply reduced to the classic MCC model.

4. The explicit stress-strain rates relationship

While the plastic ingredients of SANICLAY (e.g., yield and plastic potential functions and hence plastic hardening modulus and volume change response) may significantly be affected by the stress-induced anisotropy, constitutive equations describing the elastic branch of the behavior always remain isotropic in the original SANICALY model (see [16]). The hyper-elasticity frame has the capability to consider the influence of stress-induced anisotropy on elasticity in a natural unforced way [24]. In the following lines, the most general constitutive equations enabling the original SANICLAY to adopt anisotropic elasticity theories (including various hyper-elastic theories) are obtained.

By considering Eqs. (1) and (2), as well as Eq. (16) in Table 1, one has:

$$\begin{aligned}K_p\langle\Lambda\rangle=&K\left(\frac{\partial f}{\partial p}\right)\left(\dot{\varepsilon}_v-\langle\Lambda\rangle\frac{\partial g}{\partial p}\right)\\&+J\left(\frac{\partial f}{\partial p}\right)\left(\dot{\varepsilon}_q-\langle\Lambda\rangle\frac{\partial g}{\partial q}\right)\\&+J\left(\frac{\partial f}{\partial q}\right)\left(\dot{\varepsilon}_q-\langle\Lambda\rangle\frac{\partial g}{\partial p}\right)\\&+3G\left(\frac{\partial f}{\partial q}\right)\left(\dot{\varepsilon}_q-\langle\Lambda\rangle\frac{\partial g}{\partial q}\right).\end{aligned}\tag{18}$$

$$\Lambda = \frac{\left(J(\frac{\partial f}{\partial p})+3G(\frac{\partial f}{\partial q})\right)\dot{\varepsilon}_q+\left(K(\frac{\partial f}{\partial p})+J(\frac{\partial f}{\partial q})\right)\dot{\varepsilon}_v}{K_p+K(\frac{\partial f}{\partial p})(\frac{\partial g}{\partial p})+J\left((\frac{\partial f}{\partial p})(\frac{\partial g}{\partial q})+(\frac{\partial f}{\partial q})(\frac{\partial g}{\partial p})\right)+3G(\frac{\partial f}{\partial q})(\frac{\partial g}{\partial q})} \geq 0. \tag{19}$$

Box I

Assuming $\Lambda \geq 0$ (when plastic strains are generated, Λ gains a positive value), Eq. (19), shown in Box I, is obtained.

$J = 0$ holds in the case of isotropic elasticity for which Eq. (19) is reduced to:

$$\Lambda = \frac{3G(\frac{\partial f}{\partial q})\dot{\varepsilon}_q + K(\frac{\partial f}{\partial p})\dot{\varepsilon}_v}{K_p + K(\frac{\partial f}{\partial p})(\frac{\partial g}{\partial p}) + 3G(\frac{\partial f}{\partial q})(\frac{\partial g}{\partial q})} \geq 0. \tag{20}$$

Eqs. (18)-(20) are general and applicable to a large number of elastic-plastic constitutive models built within the MCC family. For SANICLAY model, considering Eqs. (10) and (11) yields:

$$\frac{\partial f}{\partial p} = p(N^2-\eta^2), \qquad \frac{\partial f}{\partial q} = 2p(\eta-\beta)$$

$$\frac{\partial g}{\partial p} = p(M^2-\eta^2), \qquad \frac{\partial g}{\partial q} = 2p(\eta-\alpha) \tag{21}$$

Implementing Eqs. (21) in Eq. (19) yields Eq. (22) as shown in Box II. For the case of isotropic elasticity (i.e., $J = 0$), Eq. (20) with respect to Eqs. (21) becomes:

$$\Lambda = \frac{K(N^2-\eta^2)\dot{\varepsilon}_v + 6G(\eta-\beta)\dot{\varepsilon}_q}{K_p/p+K(N^2-\eta^2)p(M^2-\eta^2)+12pG(\eta-\beta)(\eta-\alpha)} \geq 0. \tag{23}$$

Now, considering Eqs. (1) and (22), the explicit constitutive equations relating rates of stress and strain components are obtained which is shown in Box III, For media with isotropic elasticity, combining Eqs. (1) and (23) results in Eqs. (26) and (27) as shown in Box IV.

5. Evaluation of the refined model

In this section, straightforward methods for calibration of the hyper-elastic parameters (i.e., $\bar{G}$ and θ) are described first. Then, to show the influence of using hyper-elasticity theories on improvement of the predictive capacity of the SANICLAY model, the modified model simulations are compared with experimental data of four clayey soils in the following sub-sections. Parameters used by the original SANICLAY and the refined SANICLAY of this study are presented in Table 2.

5.1. The calibration procedure for $\bar{G}$ and θ

k, $\bar{G}$ and θ are parameters of the hyper-elasticity of Einav & Puzrin [24] through Eqs. (4)-(9). k can be determined from the data of unloading/reloading compression paths obtained from triaxial or oedometer tests. Considering Eq. (9), the elastic shear modulus of Einav & Puzrin [24] is reduced to $G = \bar{G}p_{\text{ref}}(p/p_{\text{ref}})^{\theta}$ under extremely low values of shear stress where p_{ref} is

Table 2. Parameters used in simulations by the refined SANICLAY of this study.

	Parameter									
Soil	M_c	M_e	N	x	C	λ	$k^{\dagger}$	$v^{\ddagger}$	$\bar{G}^{\S}$	$\theta^{\S}$
LCT	1.18	0.86	0.91	1.56	16	0.063	0.009	0.20	70	0.65
BBC	1.32	1.02	0.932	3.11	15	0.186	0.022	0.28	70	0.90
Cloverdale clay	1.29	-	1.0	1.7	3	0.21	0.03	0.20	50	0.65
AGC	1.07	0.80	0.77	2.0	25	0.282	0.049	0.20	45	0.90

†: In Eqs. (4)-(9), $\bar{k} = \frac{k}{1+e_{\text{in}}}$.

‡: Used only in the isotropic hypo-elastic constitutive equations (i.e., Eqs. (2) and (3)).

§: Used only in the hyper-elastic constitutive equations (i.e., Eqs. (1) and (4)-(9)).

$$\Lambda = \frac{(N^2-\eta^2)(K\dot{\varepsilon}_v + J\dot{\varepsilon}_q) + 2(\eta-\beta)(J\dot{\varepsilon}_v + 3G\dot{\varepsilon}_q)}{K_p/p + (N^2-\eta^2)\left[pK(M^2-\eta^2)+2pJ(\eta-\alpha)\right] + 2(\eta-\beta)\left[pJ(M^2-\eta^2)+6pG(\eta-\alpha)\right]} \geq 0. \tag{22}$$

Box II

$$\begin{Bmatrix}\dot{p}\\ \dot{q}\end{Bmatrix}=$$

$$\left[\begin{pmatrix}K & J\\ J & 3G\end{pmatrix}-\frac{h(\Lambda)}{\Re}\begin{pmatrix}pK(M^2-\eta^2)\left[K(N^2-\eta^2)+2J(\eta-\beta)\right] & pK(M^2-\eta^2)\left[J(N^2-\eta^2)+6G(\eta-\beta)\right]\\ 6pG(\eta-\alpha)\left[K(N^2-\eta^2)+2J(\eta-\beta)\right] & 6pG(\eta-\alpha)\left[J(N^2-\eta^2)+6G(\eta-\beta)\right]\end{pmatrix}\right]\times\begin{Bmatrix}\dot{\varepsilon}_v\\ \dot{\varepsilon}_q\end{Bmatrix} \quad (24)$$

where h is the Heaviside's step function: $h(\Lambda)=1$ if $\Lambda\geq 0$, and zero otherwise. $\Re$ is defined by:

$$\Re=K_p/p+(N^2-\eta^2)\left[pK(M^2-\eta^2)+2pJ(\eta-\alpha)\right]+2(\eta-\beta)\left[pJ(M^2-\eta^2)+6pG(\eta-\alpha)\right]. \quad (25)$$

Box III

$$\begin{Bmatrix}\dot{p}\\ \dot{q}\end{Bmatrix}=\left[\begin{pmatrix}K & 0\\ 0 & 3G\end{pmatrix}-\frac{h(\Lambda)}{\Re*}\begin{pmatrix}pK^2(M^2-\eta^2)(N^2-\eta^2) & 6pGK(M^2-\eta^2)(\eta-\beta)\\ 6pGK(\eta-\alpha)N^2-\eta^2) & 36pG^2(\eta-\alpha)(\eta-\beta)\end{pmatrix}\right]\times\begin{Bmatrix}\dot{\varepsilon}_v\\ \dot{\varepsilon}_q\end{Bmatrix} \quad (26)$$

where:

$$\Re*=K_p/p+pK(N^2-\eta^2)(M^2-\eta^2)+12pG(\eta-\alpha)(\eta-\beta). \quad (27)$$

Box IV

a normalizing pressure (e.g., 100 kPa). Now, G under extremely low shear stress levels can be written in the following form:

$$\log G=\log(\bar{G}p_{\rm ref})+\theta\log(p/p_{\rm ref}). \quad (28)$$

Eq. (28) indicates that θ and $\log(\bar{G}p_{\rm ref})$ are, respectively, the slope and the intercept of the best straight line fitted to the data of $\log G$ depicted versus the corresponding $\log(p/p_{\rm ref})$ values. Such experimental data are usually obtained from the resonant column or bender element tests. It is worth noting that the value of $\bar{G}$ depends on $p_{\rm ref}$ (see Eq. (28)). However identical simulations can be obtained from any arbitrary pairs ($\bar{G}_2$, $p_{\rm ref2}$) and ($\bar{G}_1$, $p_{\rm ref1}$) provided that $\bar{G}_2=\bar{G}_1(p_{\rm ref1}/p_{\rm ref2})^{1-\theta}$.

According to Viggiani & Atkinson [29] and Rampello et al. [30], θ is usually less than unity and increases with the Plasticity Index (PI). In the lack of the results of the resonant column or bender element tests, one can estimate θ by using the result of the existing data presented in Figure 5. Once θ is estimated, $\bar{G}$ can be determined by constructing tangents to the beginning parts of $q-\varepsilon_q$ curves of drained or undrained triaxial tests.

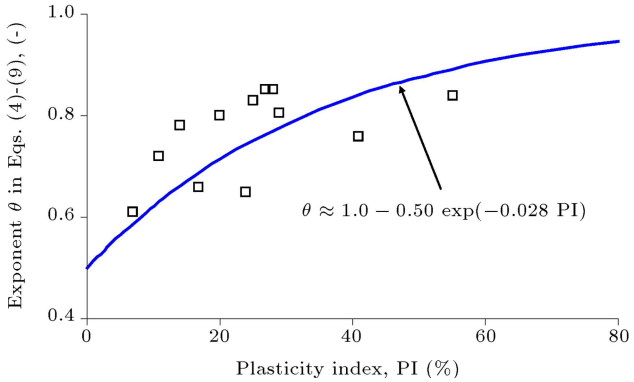

Figure 5. Variation of the exponent θ with Plasticity Index (PI) (experimental data from Viggiani & Atkinson [29] and Rampello et al. [30]).

5.2. Simulation of Lower Corner Till (LCT) behavior

Using triaxial apparatus, Gens [1] studied the mechanical behavior of normal and over-consolidated samples of LCT that is a silty clay with LL (Liquid Limit) = 25%, and PI (Plasticity Index) = 13%. Prior to shearing, samples were subjected to both isotropic (i.e., $K(=\sigma_h/\sigma_v)=1$, where σ_h and σ_v are, respectively, the horizontal and vertical effective stresses) and anisotropic (i.e., $K(=\sigma_h/\sigma_v)\neq 1$) consolidation.

For 11 samples of LCT subjected to the compression and extension modes of triaxial, an extensive series of comparisons between various models including the modified SANICLAY model of this study is presented in Figure 6. The experimental program covers a wide range of over-consolidation ratios in the range of 1-20. In parts (a) and (b) of Figure 6, predictions by the MCC model are depicted against experimental data. Considering stress paths shown in part (a), a significant

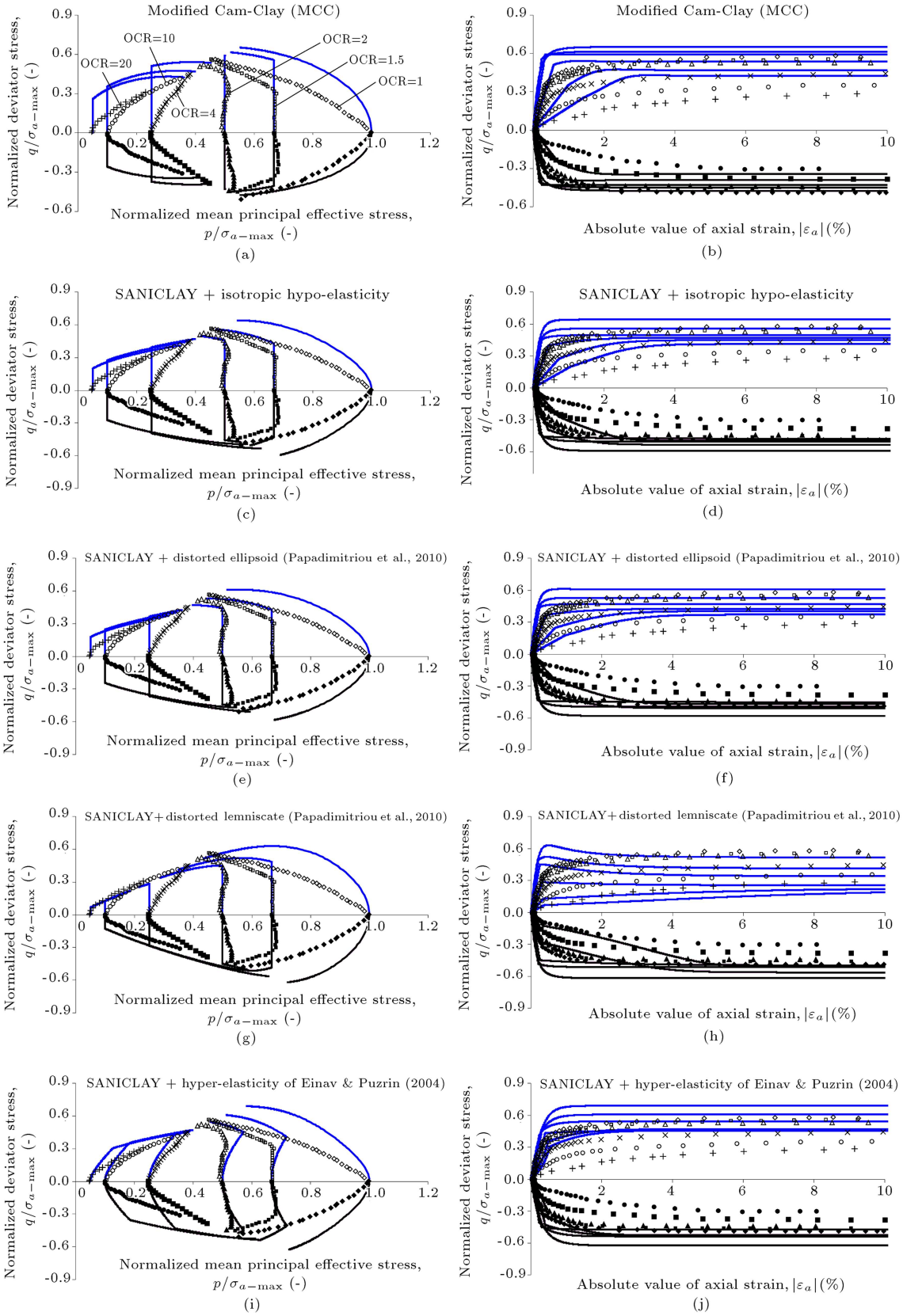

Figure 6. Comparison of experimental data of isotropically consolidated samples of LCT and predictions obtained from: (a) and (b) MCC model; (c) and (d) original SANICLAY [16]; (e) and (f) SANICLAY + distorted ellipsoid as yield function [17]; (g) and (h) SANICLAY + distorted lemniscate as yield function [17]; (*i*) and (*j*) this study: SANICLAY + hyper-elasticity of Einav & Puzrin [24] (experimental data from [1]).

deviation in the MCC model predictions from the experimental data is observed. Similar comparisons using the original SANICLAY model of [16] are shown in Figure 6(c) and (d). Compared to the MCC model predictions, a noticeable improvement for normally consolidated and lightly over-consolidated (i.e., OCR ≤ 4) is observed. However, for highly over-consolidated samples (i.e., OCR ≥ 4), the improvement is not remarkable. Having two parameters more than the original model of Dafalias et al. [16], a distorted ellipsoid is used as yield function in the refined SANICLAY model of Papadimitriou et al. [17]. Predictions obtained from the SANICLAY of Papadimitriou et al. [17] are illustrated together with the data in Figure 6(e) and (f). It can be observed that the predictions by the SANICLAY of Dafalias et al. [16] and the modified version of Papadimitriou et al. [17] are nearly identical. Another change by Papadimitriou et al. [17] concerns the selection of distorted lemniscate as yield function. Pestana & Whittle [11] were the first to suggest that distorted lemniscate can be used as yield function in soil constitutive modeling. This approach requires one new parameter compared to the original SANICLAY model. Distorted ellipsoid and distorted lemniscate yield functions are, respectively, defined by Eqs. (29) and (30) and illustrated schematically in Figures 7 and 8 (see [11,17,31]):

$$f = (q - p\beta)^2 - \left[\left(m_1 + 2(1 - m_1)\frac{p}{p_0}\right)^{m_2} N^2 - \beta^2\right] \times (pp_0 - p^2) = 0, \quad (29)$$

$$f = (q - p\beta)^2 - (m_3^2 + \beta^2 - 2\beta\eta)p^2\left[1 - \left(\frac{p}{p_0}\right)^{m_4}\right] = 0, \quad (30)$$

where, m_1, m_2, m_3 and m_4 are soil parameters. It is worth noting that Papadimitriou et al. [17] only changed the yield function while the other constitutive equations and the model parameters were identical with those of the original SANICLAY model.

In parts (g) and (h) of Figure 6, predictions calculated by the latter approach are drawn against the experiments. For those samples with OCR=1 – 4 sheared in the compression side, shear strength has a peak, which is not supported by the data. Besides, the shear strengths in the extension side are larger than the corresponding values in the compression side which is not a realistic response. Finally, for the modified model of this study, comparisons are presented in Figure 6(i) and (j). Putting side by side the previous approaches, the modified model of this study can provide more reasonable predictions particularly for samples with OCR ≥ 4.

For the eight anisotropically consolidated samples, comparisons are illustrated in Figure 9. Due

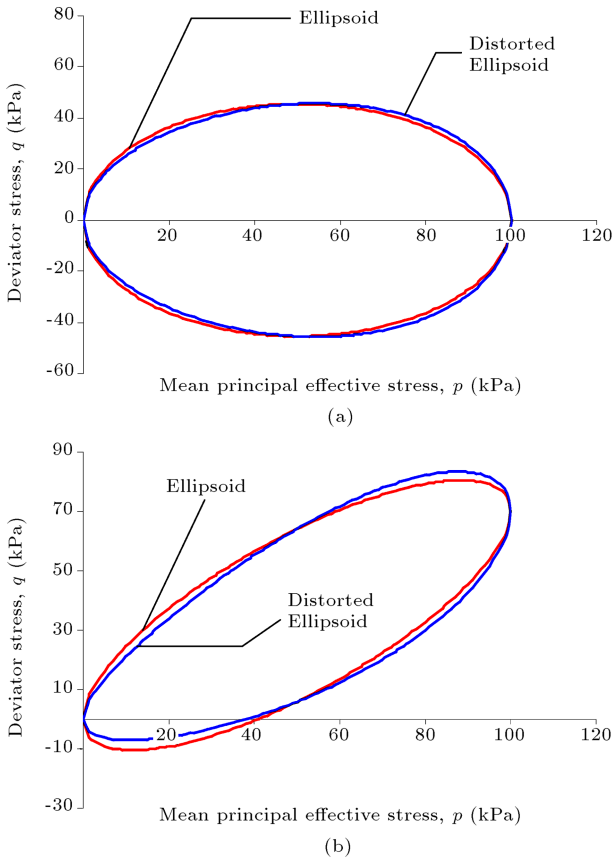

Figure 7. Illustration of ellipsoid ($N = 0.91$, $p_0 = 100$ kPa) and distorted ellipsoid ($N = 0.91$, $m_1 = 0.8$, $m_2 = 0.9$, $p_0 = 100$ kPa) yield functions: (a) Isotropic stress condition ($\beta = 0$); and (b) anisotropic stress condition ($\beta = 0.7$).

to the lack of rotational/distortional hardening in the Modified Cam-Clay (MCC) model, a remarkable deviation between predictions of this model and data occurs and thus, predictions of the MCC model are not shown in Figure 9. Similar to the last case discussed in Figure 6, the difference between the predictions of the original SANICLAY [16] and the modified SANICLAY with distorted ellipsoid [17] is negligible (see Figure 9(c) and (f)). Once again, the application of the distorted lemniscate as yield function in Papadimitriou et al. [17] leads to the weakening of predictions in Figure 9(g) and (h). Finally, simulations obtained from the modified model of this study are depicted with data in parts (i) and (j) of Figure 9. Compared to the previous cases, a concrete improvement in the simulations of stress paths is achieved.

The MCC model is incapable of considering rotational/distortional hardening required for rigorous simulation of the mechanical behavior of anisotropically consolidated samples. Therefore, in the following sub-sections, predictions by the MCC model are not included. Furthermore, predictions by the version of SANICLAY in which a distorted ellipsoid plays the

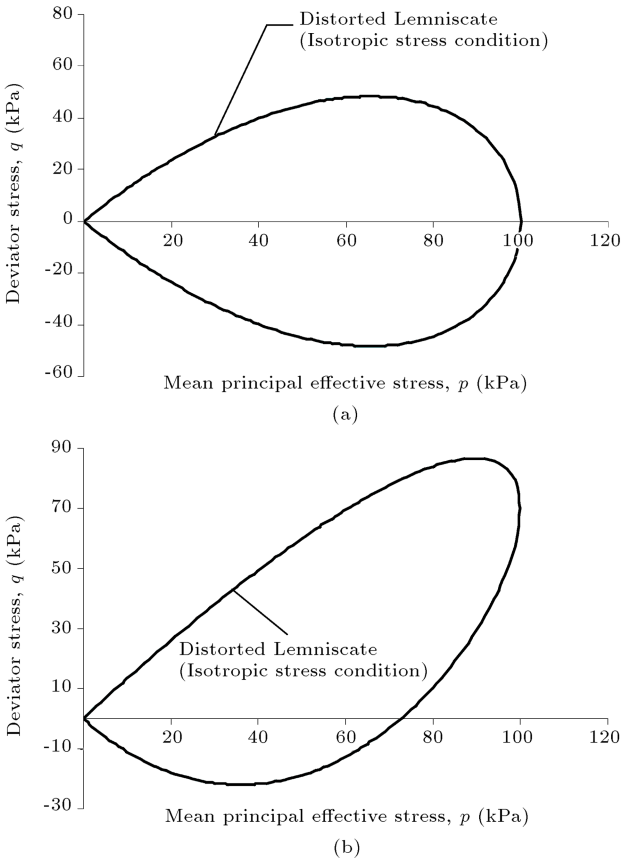

Figure 8. Illustration of distorted lemniscate ($m_3 = 1.4$, $m_4 = 0.77$, $p_0 = 100$ kPa) yield functions: (a) Isotropic stress condition ($\beta = 0$); and (b) anisotropic stress condition ($\beta = 0.7$).

role of yield function are nearly identical to those of the original SANICLAY. Besides, it has been observed that using distorted lemniscates as yield function in the SANICLAY platform results in undesirable simulations. Considering these points, the predictive capacity of the latter versions of SANICLAY is not discussed in sequel.

By using the same parameters obtained for simulation of the tests presented in Figures 6 and 9, the mechanical behavior of anisotropically consolidated samples of LCT is simulated here. In Figure 10, predictions by the modified SANICLAY model of this study are depicted against experimental data of 7 undrained tests of isotropically and anisotropically consolidated samples of LCT with OCR=1. Similar comparisons under drained condition are conducted in Figure 11.

Through Figures 6 and 9-11, a noticeable improvement in simulation of stress paths was obtained. However, the modified model predictions for deviator stress versus deviator strain response were less favorable due to the unrealistic increase in shear stiffness for highly over-consolidated samples. A possible reason for this deficiency is discussed in Section 6.

In the original SANICLAY model, the initial void ratio is calculated by using normal compression line in conjunction with elastic unloading/reloading lines. The Gibbs free energy function, Eq. (4), leads to a linear unloading/reloading lines in $e - \ln p$ plane identical to that of the conventional critical state soil mechanics [24]. As a result, the initial void ratio in the modified model can be calculated similar to that of the original SANICLAY. Alternatively, stress state may be set to $(p, q) = (p_0, q_0)$ and then unloaded to $(p_{\text{in}}, q_{\text{in}})$ within the yield function using the hyper-elastic model. The first approach is followed in this study. Finally, it is worth noting that a number of triaxial tests shown in Figures 9, 12, 13, and 15 were conducted after K_0-unloading. For these tests, the desired initial stress states are assigned in the computer codes used for prediction of the experiments. Simulation of a K_0-unloading test is discussed in Sub-section 5.6.

5.3. Simulation of Boston Blue Clay (BBC) behavior

The physical and the mechanical properties of BBC, a natural low plasticity marine clay of moderate sensitivity (LL = 42%, PI = 21%, and S (Sensitivity) = 3 ∼7), have been extensively studied at Massachusetts Institute of Technology (MIT), and various construction projects in the region (e.g., [2-4]). Experiments are mainly conducted on anisotropically consolidated samples in order to replicate the in-situ state of stress. For 7 tests reported by Ladd & Varallyay [2] and Fayad [3], the mechanical behaviors are simulated by the original SANICLAY and the modified SANICLAY of this study and the results are compared with the corresponding experimental data in Figure 12. Sheahan [4] conducted a series of experiments on BBC clay sheared in the compression side. Evaluations of the original and modified SANICLAY models against this set of data are presented in Figure 13. Comparison of predictions with experiments shown through Figures 12 and 13 reveals that a tangible improvement is achieved when conservation of energy in elasticity is taken into account.

In simulation of the mechanical behavior of BBC clay, $M_e > N$ is noticeable. The use of $M_e > N$ may potentially lead to a softening response in undrained triaxial extension, following anisotropic consolidation towards the compression side; this especially occurs if the C value is low.

5.4. Simulation of Cloverdale clay behavior

Zergoun [5] and Zergoun & Vaid [6] studied the mechanical behavior of Cloverdale clay under triaxial condition. Cloverdale clay is a sensitive undisturbed marine silty clay with LL = 50%, PI =24%, A (Activity) = 0.55, and S = 16. In Figure 14, behaviors of three isotropically consolidated samples of Cloverdale clay

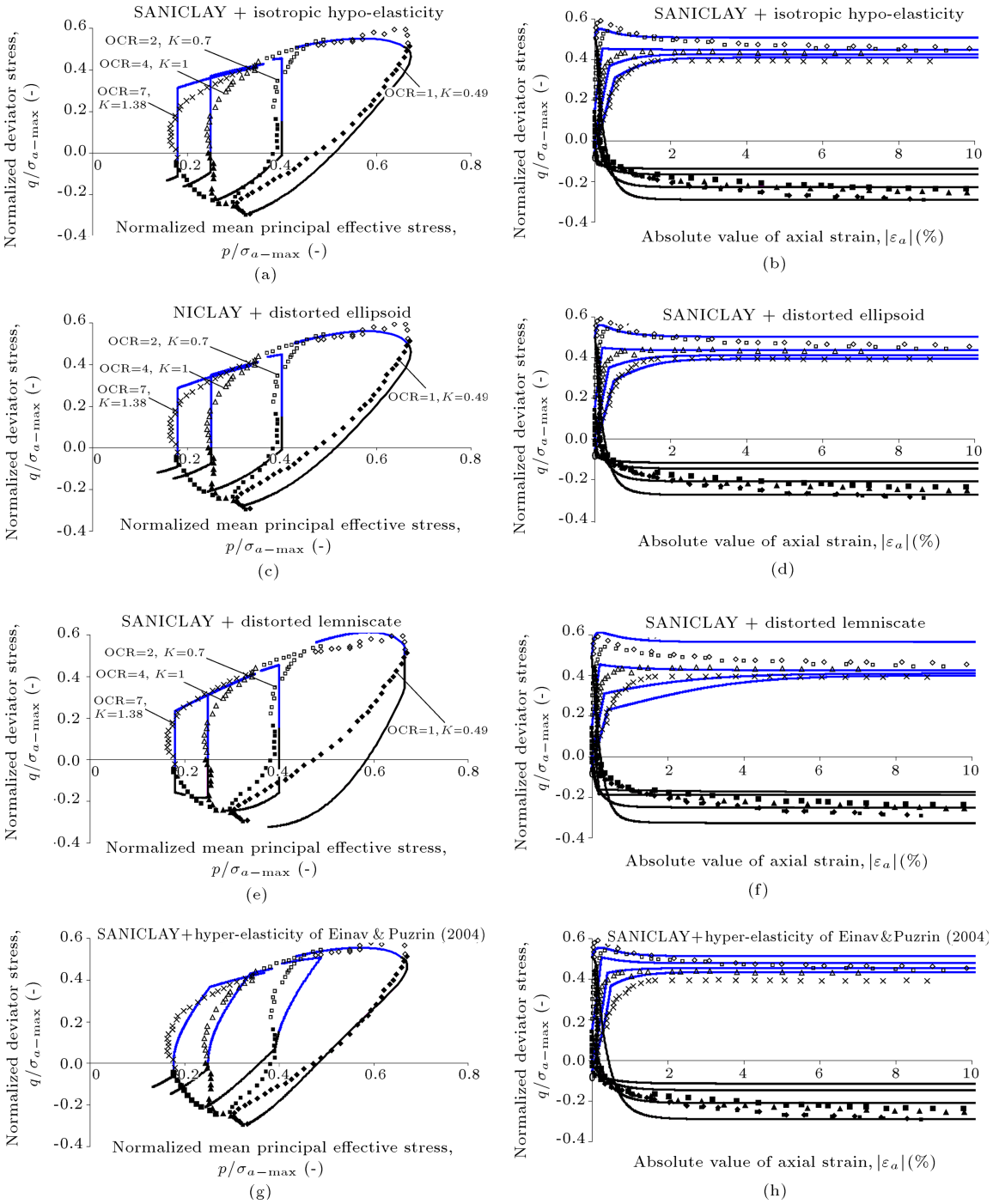

Figure 9. Comparison of experimental data of anisotropically consolidated samples of LCT and predictions obtained from: (a) and (b) the original SANICLAY [16]; (c) and (d) SANICLAY + distorted ellipsoid as yield function [17]; (e) and (f) SANICLAY + distorted lemniscate as yield function [17]; (g) and (h) this study: SANICLAY + hyper-elasticity of Einav & Puzrin [24] (experimental data from [1]).

are simulated using the original SANICLAY and the modified SANICLAY of this study. It can be observed that the modified model gives more realistic predictions for moderate-large over-consolidated (OCR = 2.1, and 3.3) samples.

It is worth noting that only the mechanical behavior of Cloverdale clay subjected to the compression mode of triaxial is studied in [5,6] and hence, M_e is not reported in Table 2.

5.5. Simulation of Average Gulf Clay (AGC)

For five major groundwater projects in the Gulf of Mexico, the mechanical behavior of lower Pleistocene deposits have been studied [7,32]. Deposits are mainly

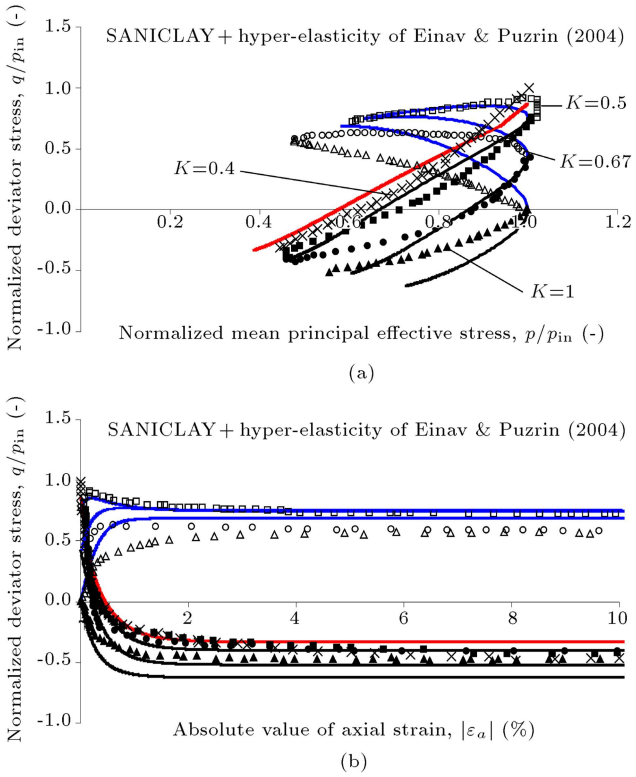

Figure 10. Comparison of undrained experimental data of anisotropically consolidated samples of LCT under OCR=1, and predictions obtained from the model of this study: SANICLAY + hyper-elasticity of Einav & Puzrin [24] (experimental data from [1]).

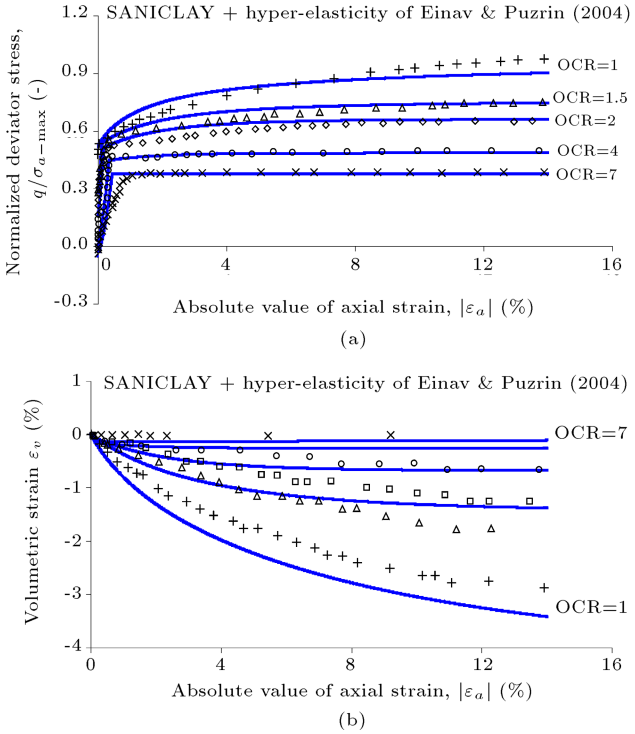

Figure 11. Comparison of drained experimental data of anisotropically consolidated samples of LCT under various OCR values and predictions obtained from the model of this study: SANICLAY + hyper-elasticity of Einav & Puzrin [24] (experimental data from [1]).

clay sediments with PI=60 $\sim$ 40% for samples taken from depths 30 and 150 m, respectively, and S $\approx$ 2. For 7 anisotropically consolidated samples taken from 5 sites, predictions by the original and the refined SANICLAY models are compared with data in Figure 15. It can be observed that the modified model gives more realistic predictions for the over-consolidated samples.

5.6. Simulation of K_0-unloading

When subjected to K_0-unloading, clay behavior is primarily elastic. As a result, K_0-unloading is suitable for evaluation of constitutive equations describing the elastic response of clayey soils. By using Eq. (1), stress increments under K_0-unloading become:

$$\dot{p} = (2G + J)\dot{\varepsilon}_1^e; \qquad \dot{q} = (K + 2/3J)\dot{\varepsilon}_1^e. \tag{31}$$

For the original SANICLAY with isotopic hypo-elasticity, G and K are given in Eq. (3), and $J = 0$. For the case of modified SANICLAY of this study with hyper-elasticity, G, J, and K can be found in Eq. (8). Simulations by isotropic hypo-elastic and hyper-elastic models are depicted against experimental data in Figure 16. A slightly better agreement between the hyper-elastic model simulation and the experimental data can be observed in the figure.

5.7. The model normalized response

According to the conventional critical state soil mechanics (e.g., [20]), the mechanical behavior of reconstituted clayey soils subjected to either drained or undrained triaxial shearing can be normalized with respect to the pre-consolidation stress. The mechanical behavior predicted by both the MCC and SANICLAY models can be normalized with respect to p_0 as a direct consequence of the linear dependence of K and G on p. Recent experimental findings have indicated that K of clays varies linearly with p; however, G changes with $(p/p_{ref})^{\theta}$ (e.g., [29,30]). θ is usually less than unity and changes with Plasticity Index (PI); see Figure 5. The hyper-elastic theory of Einav & Puzrin [24] can take into account the latter observation. Nevertheless, a unique normalized response may not be obtained by implementation of the hyper-elastic theory of Einav & Puzrin [24] in the MCC or SANICLAY frameworks. In parts (a) and (b) of Figure 17, the normalized predicted response of four tests on normally consolidated samples (OCR=1) with p_{in} = 100, 200, 400 and 1000 kPa are presented for the $\theta = 0.65$ case. For four highly over-consolidated samples (OCR=4), a similar comparison is presented in Figure 17(c) and (d). Figure 17 indicates that the difference between the critical state strength of the samples with p_{in} = 100 and 1000 kPa is less than 7%. Mathematically the

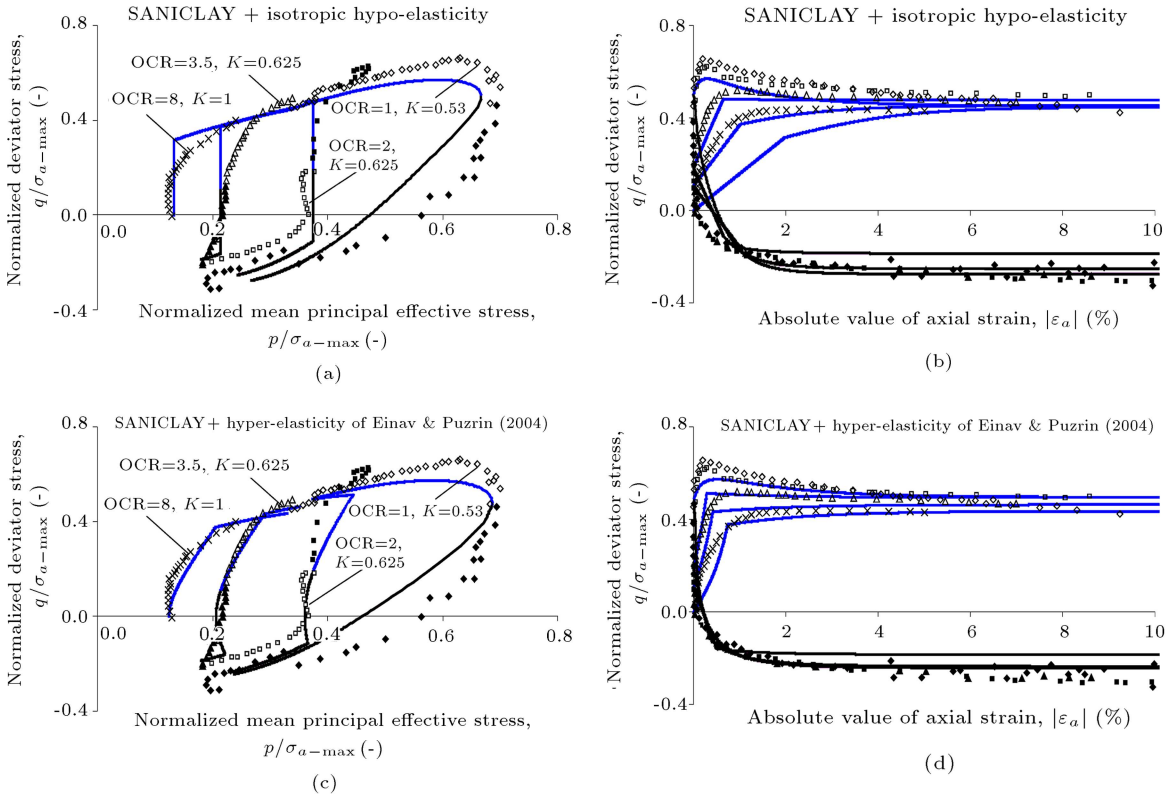

Figure 12. Experimental data of anisotropically consolidated samples of BBC versus predictions obtained from: (a) and (b) the original SANICLAY [16]; (c) and (d) this study: SANICLAY + hyper-elasticity of Einav & Puzrin [24] (experimental data from [2,3]).

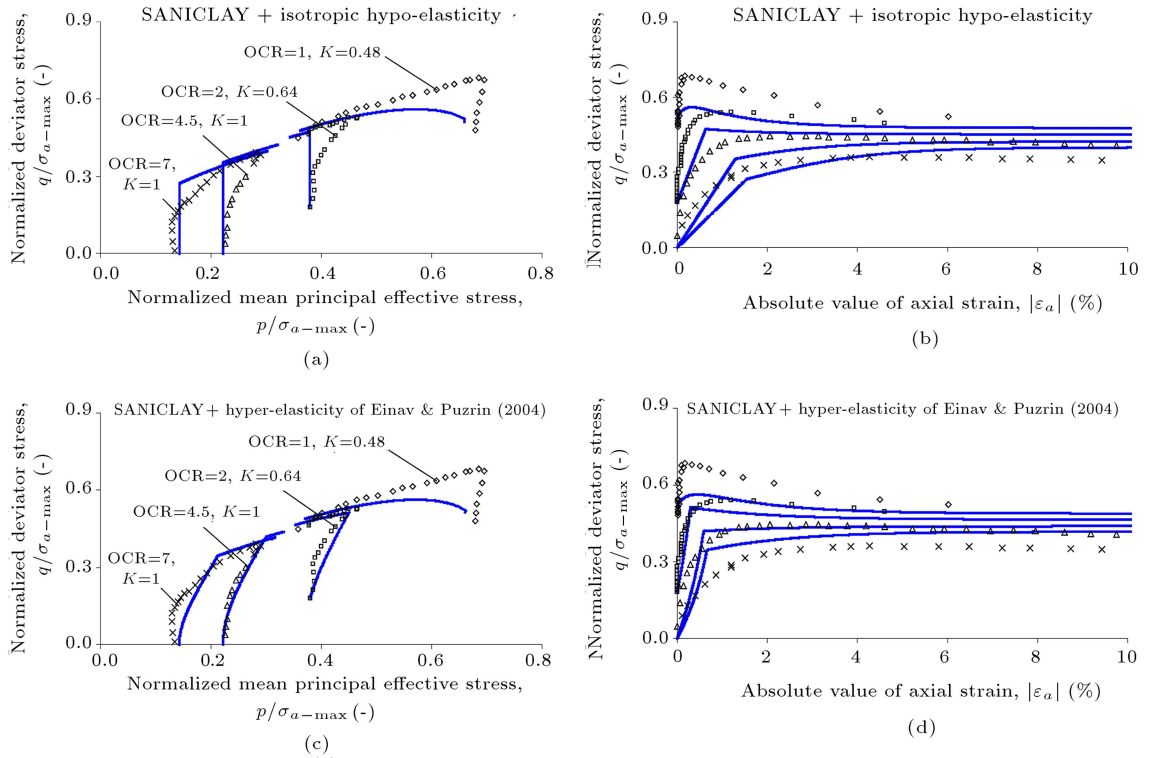

Figure 13. Experimental data of anisotropically consolidated samples of BBC versus predictions obtained from: (a) and (b) the original SANICLAY [16]; (c) and (d) this study: SANICLAY + hyper-elasticity of Einav & Puzrin [24] (experimental data from [4]).

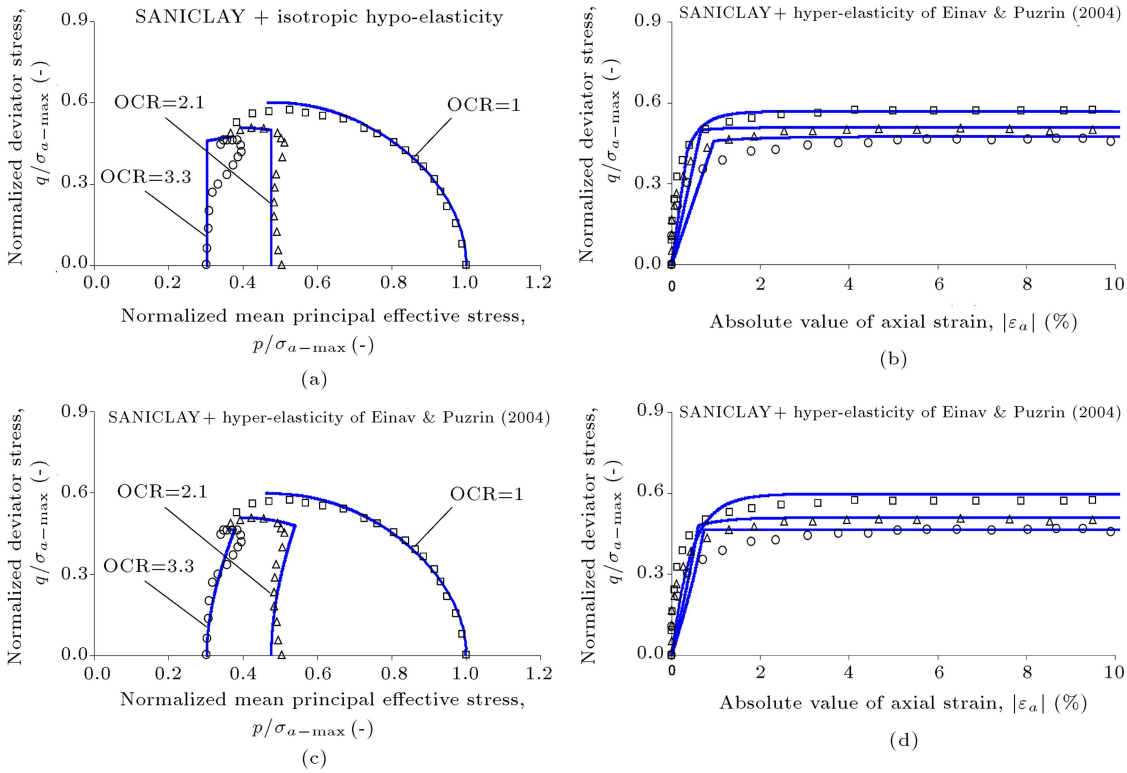

Figure 14. Experimental data of isotropically consolidated samples of Cloverdale clay versus predictions obtained from: (a) and (b) the original SANICLAY [16]; (c) and (d) this study: SANICLAY + hyper-elasticity of Einav & Puzrin [24] (experimental data from [5]).

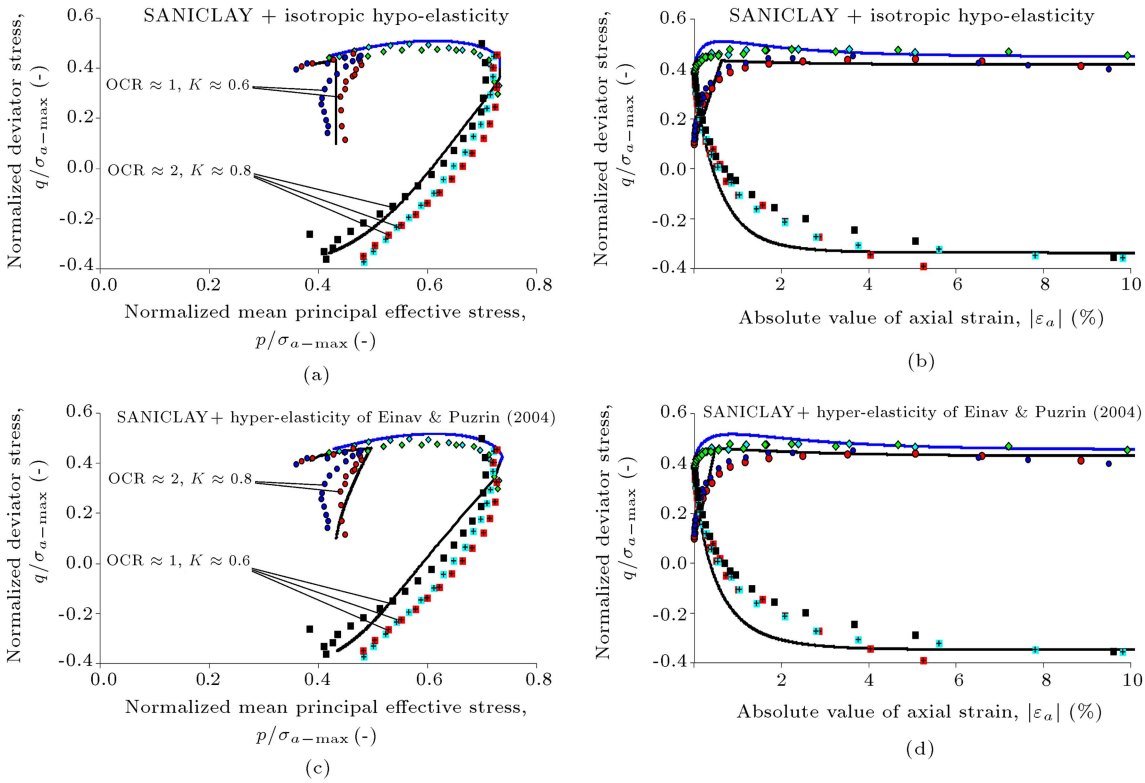

Figure 15. Experimental data of anisotropically consolidated samples of AGC versus predictions obtained from: (a) and (b) the original SANICLAY [16]; (c) and (d) this study: SANICLAY + hyper-elasticity of Einav & Puzrin [24] (experimental data from).

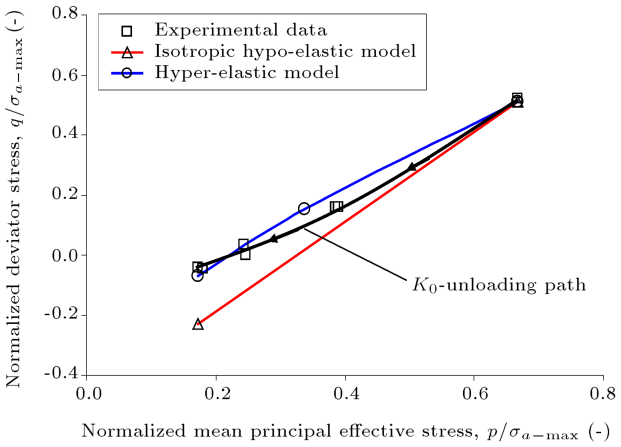

Figure 16. Simulation of a K_0-unloading path of a LCT sample using the isotropic hypo-elastic model ($v = 0.2$) and the hyper-elastic model.

mechanical response may not be normalized; however, from a practical view the disparity is not larger than that of the conventional experimental data. For each simulation shown in Figure 17, the initial void ratio was calculated by means of normal compression and elastic unloading-reloading lines in conjunction with the initial value of mean principal effective stress.

6. Conclusions

The SANICLAY model in its original form employs ellipsoid constitutive surfaces. Recent attempts to improve the predictive capacity of SANICLAY by changing the shape of its yield/plastic potential functions have been disappointing. For example, it has been shown that the implementation of yield functions in the shape of distorted lemniscate does not result in favorable simulations. Besides, the application of yield function in the shape of distorted ellipsoid results in a minor improvement in simulations. However, considering that the latter approach requires two parameters more compared to the original platform, the progress may become trivial.

Elastic strains are obtained from an isotropic hypo-elastic model in previous SANICLAY models. This assumption ignores the influence of anisotropy on elasticity and does not guarantee to conserve energy. It is clear that both outcomes are unattractive.

In this study, constitutive equations of the SANICLAY platform were generalized in order to enable it to consider the possibility of the anisotropic response of the elasticity. The generalized formulation allows shear-volumetric coupling that does not exist in the

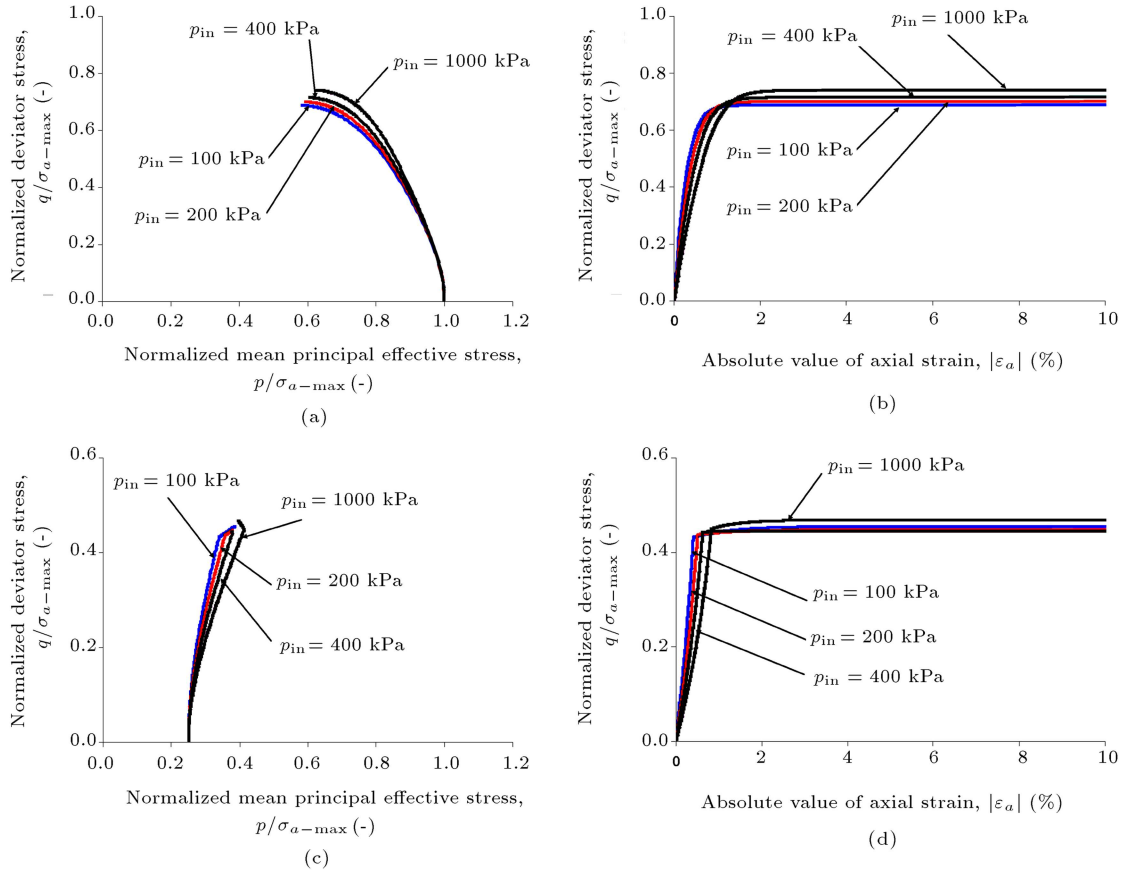

Figure 17. Numerical studies regarding the influence of initial stress state on the predicted response: (a) and (b) normally consolidated samples (OCR=1); (c) and (d) highly over-consolidated samples (OCR=4).

basic platform. Elastic strains were calculated, afterwards, using a hyper-elastic model proper for cohesive soils. As a result, the following benefits were realized:

- The conservation of energy is guaranteed in purely elastic domain of behavior and as a direct consequence, elastic strains are fully recoverable.
- The model performance was evaluated against 52 tests on four different types of clayey soils. For moderately to highly over-consolidated samples, a noticeable improvement in simulated stress paths was observed.
- The influence of stress-induced anisotropy on the elastic portion of the behavior is taken into account in a natural unforced way. In the modified model, both the elastic and plastic ingredients are affected consistently by stress-induced anisotropy.

Compared to the original framework, the modified model requires one new parameter (i.e., θ) for calculation of the pressure-dependent elastic shear modulus of clays. While a noticeable improvement in simulation of stress paths was obtained, the modified model predictions for deviator stress versus deviator strain response were less favorable due to the unrealistic increase in shear stiffness for highly over-consolidated samples. In SANICLAY platform, the elastic and plastic strain rates were calculated independently; however, it is known that the elastic and plastic branches of the mechanical behavior of geomaterials are coupled [33-38]. For sands, it has been shown that considering the elastic-plastic coupling may lead to the improvement of predictions (e.g., [36-38]). In this regard, considering the influence of over-consolidation on the elastic moduli of clays should be studied in future studies.

Acknowledgment

The authors wish to acknowledge anonymous reviewers for constructive comments. The authors are also thankful to Dr. Ehsan Seyedi Hosseininia of Ferdowsi University of Mashhad, Mr. Behtash Javidsharifi of Shiraz University of Technology, and Dr. Banafsheh Lashkari of Shiraz University for their critical review of the manuscript.

References

1. Gens, A. "Stress-strain and strength of low plasticity clay", Ph.D. Thesis, Imperial College, London University, England (1982).
2. Ladd, C.C. and Varallyay, J. "The influence of the stress system on the behavior of saturated clays during undrained shear", *Research Report No. R65-11.*, Department of Civil Engineering, MIT, Cambridge, MA, USA (1965).
3. Fayad, P. "Aspects of the volumetric and undrained behavior of Boston blue clay", SM Thesis, Department of Civil and Environmental Engineering, MIT, Cambridge, MA, USA (1986).
4. Sheahan, T.C. "An experimental study of the time-dependent undrained shear behavior of resedimented clay using automated stress-path triaxial equipment", Sc.D. Thesis, Department of Civil and Environmental Engineering, MIT, Cambridge, MA, USA (1991).
5. Zergoun, M. "Effective stress response of clay to undrained cyclic loading", Ph.D. Thesis, the University of British Columbia, Vancouver, British Columbia, Canada (1991).
6. Zergoun, M. and Vaid, Y. "Effective stress response of clay to undrained cyclic loading", *Canadian Geotechnical Journal*, **31**(5), pp. 714-727 (1994).
7. Whittle, A.J. and Sutabutr, T. "Parameters for average gulf clay and prediction of pile set-up in the Gulf of Mexico", *Soil Constitutive Models: Evaluation, Selection, and Calibration. ASCE Geotechnical Special Publication*, No. 128, Yamamuro, J.A. and Kaliakin, V.N., Eds., pp. 440-458 (2005).
8. Roscoe, K.H. and Burland, J.B. "On the generalised stress-strain behaviour of wet clay", *Engineering Plasticity*, Heyman, J. and Leckie, F.A., Eds., Cambridge University Press, pp. 535-609 (1968).
9. Dafalias, Y.F. "An anisotropic critical state soil plasticity model", *Mechanics Research Communications*, **13**(6), pp. 341-347 (1986).
10. Newson, T.A. and Davies, M.C.R. "A rotational hardening constitutive model for anisotropically consolidated clay", *Soils and Foundations*, **36**(3), pp. 13-20 (1996).
11. Pestana, J.M. and Whittle, A.J. "Formulation of a unified constitutive model for clays and sands", *International Journal for Numerical and Analytical Methods in Geomechanics*, **23**(12), pp. 1215-1243 (1999).
12. Wheeler, S.J., Näätänen, A., Karstunen, M. and Lojander, M. "An anisotropic elastoplastic model for soft clays", *Canadian Geotechnical Journal*, **40**(2), pp. 403-418 (2003).
13. Karstunen, M., Wiltafsky, C., Krenn, H., Scharinger, F. and Schweiger, H.F. "Modelling the behaviour of an embankment on soft clay with different constitutive models", *International Journal for Numerical and Analytical Methods in Geomechanics*, **30**(10), pp. 953-982 (2006).
14. Dafalias, Y.F., Manzari, M.T. and Akaishi, M. "A simple anisotropic clay plasticity model", *Mechanics Research Communications*, **29**(4), pp. 241-245 (2002).
15. Ling, H.I., Yue, D., Kaliakin, V.N. and Themelis, N.J. "Anisotropic elastoplastic bounding surface model for cohesive soils", *ASCE Journal of Engineering Mechanics*, **128**(7), pp. 748-758 (2002).
16. Dafalias, Y.F., Manzari, Y.F. and Papadimitriou, A.G. "SANICLAY: simple anisotropic clay plasticity

model", *International Journal for Numerical and Analytical Methods in Geomechanics*, **30**(12), pp. 1231-1257 (2006).

17. Papadimitriou, A.G., Vranna, A.D., Dafalias, Y.F. and Manzari, M.T. "Effect of yield surface shape on the simulated elasto-plastic response of cohesive soils", *Numerical Methods in Geotechnical Engineering*, Benz & Nordal, Eds., Taylor & Francis Group, pp. 63-68 (2010).
18. Taiebat, M., Dafalias, Y.F. and Peek, R. "A destructuration theory and its application to SANICLAY model", *International Journal for Numerical and Analytical Methods in Geomechanics*, **34**(10), pp. 1009-1040 (2010).
19. Simpson, B. "Finite elements applied to problems of plain strain deformation in soil", Ph.D. Thesis, University of Cambridge, Cambridge, England (1973).
20. Atkinson, J.H., *Foundations and Slopes: An Introduction to Applications of Critical State Soil Mechanics*, John Wiley & Sons, New York, USA (1981).
21. Gens, A. and Potts, D.M. "Critical state models in computational geomechanics", *Engineering Computations*, **5**, pp. 178-197 (1988).
22. Zytynski, M., Randolph, M.F., Nova, R. and Wroth, P. "On modelling the unloading-reloading behaviour of soils", *International Journal for Numerical and Analytical Methods in Geomechanics*, **2**, pp. 87-93 (1978).
23. Borja, R.I., Tamagnini, C. and Amorosi, A. "Coupling plasticity and energy-conserving elasticity models for clays", *ASCE Journal of Geotechnical and Geoenvironmental Engineering*, **123**(10), pp. 948-057 (1997).
24. Einav, I. and Puzrin, A.M. "Pressure-dependent elasticity and energy conservation in elastoplastic models for soils", *ASCE Journal of Geotechnical and Geoenvironmental Engineering*, **130**(1), pp. 81-92 (2004).
25. Houlsby, G.T., Amorosi, A. and Rojas, E. "Elastic moduli of soils dependent on pressure: A hyperelastic formulation", *Géotechnique*, **55**(5), pp. 383-392 (2005).
26. Graham, J. and Houlsby, G.T. "Anisotropic elasticity of a natural clay", *Géotechnique*, **33**(2), pp. 165-180 (1983).
27. Muir Wood, D., *Soil Behavior and Critical State Soil Mechanics*, Cambridge University Press, USA (1990).
28. Lashkari, A. "A SANISAND model with anisotropic elasticity", *Soil Dynamics and Earthquake Engineering*, **30**, pp. 1462-1477 (2010).
29. Viggiani, G., Atkinson, J.H. "Stiffness of fine-grained soil at very small strains", *Géotechnique*, **45**(2), pp. 249-265 (1995).
30. Rampello, S., Viggiani, G.M.B. and Amorosi, A. "Small-strain stiffness of reconstituted clay compressed along constant triaxial effective stress ratio paths", *Géotechnique*, **47**(3), pp. 475-489 (1997).
31. Taiebat, M. and Dafalias, Y.F. "Simple yield surface expressions appropriate for soil plasticity", *ASCE International Journal of Geomechanics*, **10**(4), pp. 161-169 (2010).
32. Quiros, G.W., Young, A.G., Pelletier, J.H. and Chan, J.H.C. "Shear strength interpretation for Gulf of Mexico clays", *ASCE Proc. Geotechnical Practice in offshore Engineering*, Austin, TX, USA (1983).
33. Hueckel, T. "Coupling of elastic and plastic deformation of bulk solids", *Meccanica*, **11**, pp. 227-235 (1976).
34. Hueckel, T., Tutumluer, E. and Pellegrini, R. "A note on non-linear elasticity of isotropic overcosolidated clays", *International Journal for Numerical and Analytical Methods in Geomechanics*, **16**, pp. 603-618 (1992).
35. Collins, I.F. and Houlsby, G.T. "Application of thermomechanical principles to the modeling of geotechnical materials", *Proceedings of Royal Society A*, **453**, pp. 1975-2001 (1997).
36. Lashkari, A. and Golchin, A. "On the influence of elastic-plastic coupling on sands response", *Computers and Geotechnics*, **55**, pp. 352-364 (2014).
37. Golchin, A. and Lashkari, A. "A critical state sand model with elastic-plastic coupling", *International Journal of Solids and Structures*, **51**, pp. 2807-2825 (2014).
38. Lashkari, A. "Prediction of flow liquefaction instability of clean and silty sands", *Acta Geotechnica* (2015) (In press). DOI 10.1007/s11440-015-0413-9.

Biographies

Ali Lashkari was born in 1977. He received his PhD degree in Geotechnical Engineering from Tehran University in 2007. Dr. Lashkari is currently Associate Professor in the Department of Civil & Environmental Engineering at Shiraz University of Technology. His main research interest is the mechanics of constitutive equations in soils including modeling of the anisotropic aspects of soils behavior, constitutive modeling of liquefaction, simulation of the mechanical behavior of soil-structure interfaces, unsaturated soil mechanics, and micromechanics.

Meisam Mahboubi was born in 1989 in Lahidjan, Guilan, Iran. He received his BS degree in Civil Engineering from Mahaghegh-e-Ardebilli University in 2011, and his MSc degree in Geotechnical Engineering from Shiraz University of Technology in 2013. His research interests are mainly fundamental subjects in Geomechanics including the application of the elasto-plasticity theory in constitutive modeling of clays and bearing capacity of rock foundations. He is also author and co-author of several publications.